MODELING OF UPPER STAGE CRYOGENIC PROPELLANT STRATIFICATION IN A ROTATING, REDUCED GRAVITY ENVIRONMENT

Mark D. Ratner[1], Fumitaka Goto[1] and Daniel R. Kirk[2]
Mechanical and Aerospace Engineering Department
Florida Institute of Technology

Paul A. Schallhorn[3]
Expendable Launch Vehicle / Mission Analysis Branch
NASA John F. Kennedy Space Center

Abstract

Payloads requiring insertion into high altitude orbits are delivered using the upper stages of chemical rockets (ex., Delta and Atlas classes) normally employing cryogenic propellants. During the transfer period between orbits, the upper stage may coast for several hours during which time the thermodynamic state of the propellants may vary due to solar heating. At the conclusion of the coast phase, and in preparation for orbital insertion of the payload, the propellants must be within a narrowly defined range of temperature and pressure for the engine to resume operation. Therefore it is vital to ensure that the propellants are within the specified thermodynamic boundaries or the engine may not restart, resulting in mission failure. This paper investigates several simplified analytical and computational models which are used to predict the state of the propellants at the conclusion of a low to high earth orbit coast phase.

1. Introduction

For pump-fed, chemical engines to operate properly sufficient tank inlet pressure is required to suppress cavitation in the pump. Solar heating during orbital transfer may result in thermally stratifying the cryogenic propellants prior to upper stage engine re-start. The thermodynamic state of the propellant may vary within the tank, and if the propellant drawn into the turbomachinery is outside a specified temperature and pressure bound the engine may not function. Therefore it is critical to predict the propellant state at the conclusion of the coast phase and a sufficiently detailed model of thermal stratification is essential, [1, 8, 11]. Table 1 summarizes the range of parameters for the current study.

Table 1: Summary of Parameter Ranges

Parameter	Range of Parametric Investigation
Fluids: Propellants and Cryogens	LH_2, LOX, LN_2, LH_2O
LH_2 Bulk Temperature, $T_{B,LH2}$, [K, R]	$15\ K \le T_{B,LH2} \le 20\ K$, $27\ R \le T_{B,LH2} \le 36\ R$
LOX Bulk Temperature, $T_{B,LOX}$, [K, R]	$90\ K \le T_{B,LOX} \le 110\ K$, $162\ R \le T_{B,LOX} \le 198\ R$
Driving Temperature Gradient, ΔT, [K, ºF]	$0.1\ K \le \Delta T \le 4\ K$, $0.05\ ºF \le \Delta T \le 7\ ºF$
Reduced Gravity Level, g/g_0	$10^{-5} \le g/g_0 \le 1$
Spin Rate, ω, [degrees/s]	$0.1º/s \le \omega \le 10º/s$
Propellant Tank Geometry	Cylindrical with spherical and elliptical end caps representative of upper stage tank geometries
Initial Tank Fill Volume, $Vol_{prop,initial}$	$10\ \% \le Vol_{prop,initial} \le 50\ \%$
Simulated Coast Duration	1 – 4 Hours

[1] Graduate Research Assistant
[2] Assistant Professor, Mechanical and Aerospace Engineering
[3] Expendable Launch Vehicle / Mission Analysis Branch - Thermal/Fluids Team Lead

Some of the physical phenomena taking place inside the cryogenic propellant tanks include a microgravity environment, incident solar heat loads, thermal conditioning (usually accomplished by spinning the spacecraft about its longitudinal axis), buoyancy induced recirculation, molecular diffusivity between propellants and corresponding pressurants, thermal conduction within the propellant and tank walls, and surface tension effects. This work develops simplified analytical and computational models to explore the stratified thermodynamic state of fluids over a range of conditions for cryogenic hydrogen, oxygen, nitrogen and liquid water. A schematic representation of the propellant tank, as well as some of the important physical processing taking place, is shown in Figure 1.

2. Reduced Order Analytical Modeling

Accurate modeling of the propellants requires an understanding of the mechanisms by which energy and mass are transported within the tank. The principal mechanism is buoyancy-induced natural convection which is initiated by solar heating of the tank walls. The walls warm the adjacent fluid and lower its density. Mass is entrained into the free-convection boundary layer that grows along the inner walls of the tank and is transported to the upper region of the cold bulk fluid forming a thermally stratified layer. The primary parameter used to classify flows of this type is the non-dimensional Rayleigh number, Ra, which is a product of the Grashof number, Gr (ratio of buoyant force to viscous force), and Prandtl number, Pr:

$$Ra = Gr\,\mathrm{Pr} = \frac{g\beta\Delta T L^3}{\nu^2}\frac{\mu c_p}{\kappa} \qquad 1$$

The ΔT is defined as the difference between the wall temperature, T_w, and the cold fluid bulk temperature, T_b. Some of these details are also shown in Figure 1.

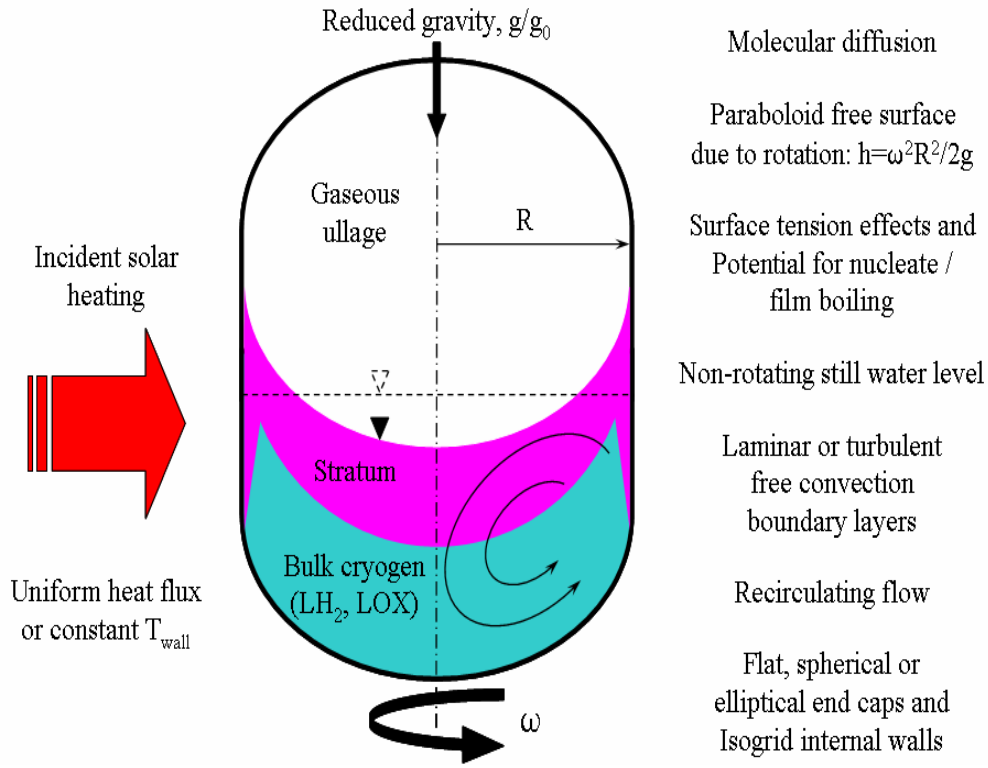

Figure 1: Schematic of cryogenic propellant tank and associated physical phenomena

Boundary layer development within the tank is assumed to begin at the bottom edge of the tank wall. Typically the boundary layer will transition to turbulence around Ra~10^9 and Equation 1 may be used to solve for the transition distance along the tank wall. For simplicity, the boundary layer is taken to be either laminar or turbulent. Figure 2 shows a non-dimensional map of Rayleigh number vs. reduced gravity ratio, g/g_0, as a function of wall and bulk temperature difference for liquid hydrogen, with the flow below and above the horizontal Ra=10^9 line corresponding to laminar and turbulent boundary layers, respectively.

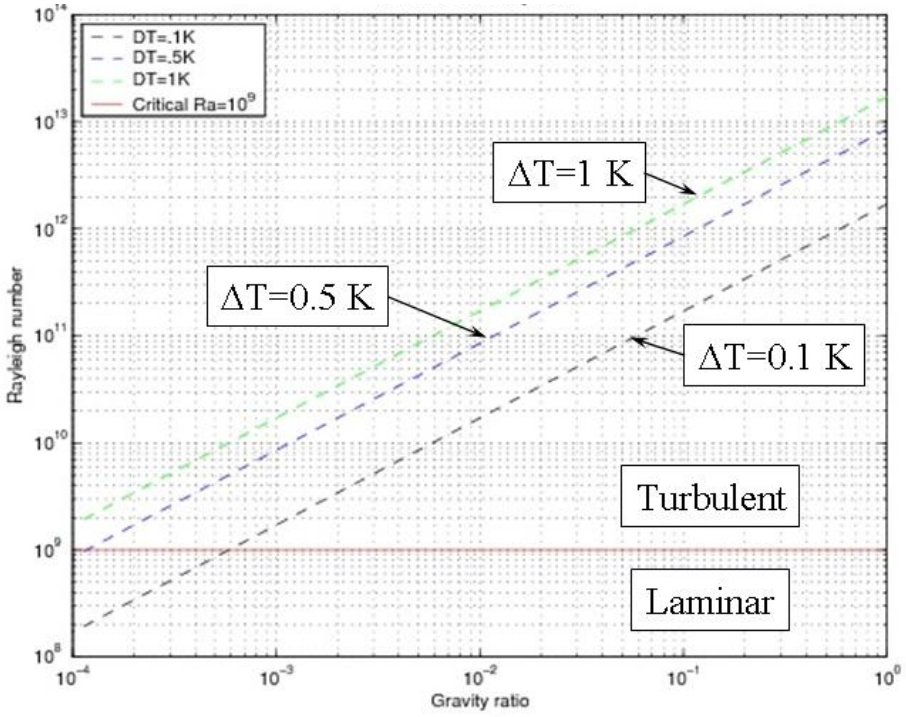

Figure 2: Example of non-dimensional map of Ra vs. reduced gravity ratio, g/g_0, for range of parameters for which boundary layer flow will be turbulent or laminar for LH_2

Behavior of the free convection boundary layer has been analyzed in detail by Eckert [3] by comparing free convection flow to a forced convection case of the same geometry. The turbulent velocity and temperature profiles are:

$$u = u_1 (y/\delta)^{1/7}(1-y/\delta)^4 \qquad u_1 = 1.185\frac{\nu}{x} Gr^{1/2}(1+0.494\,\mathrm{Pr}^{2/3})^{-1/2} \qquad 2$$

$$\theta = \theta_w(1-(y/\delta)^{1/7}) \qquad \delta = .565 x Gr^{-1/10}\,\mathrm{Pr}^{-8/15}(1+0.494\,\mathrm{Pr}^{2/3})^{1/10} \qquad 3$$

These expressions for the boundary layer velocity and temperature profiles are the basis for other models found in the literature, [1, 11]. Eckert also correlates Nusselt numbers for both laminar and turbulent regimes by comparison to experimental data:

$$Nu = CGr^{2/5}\,\mathrm{Pr}^{7/15}(1+0.494\,\mathrm{Pr}^{2/3})^{-2/5} \qquad C_{turb}=0.0295 \text{ and } C_{lam}=0.0246 \qquad 4$$

Using Eckert as a basis for a thermal stratification model, Bailey [1] combines the expressions of integral mass and energy balances into the boundary layer. This model assumes that heat enters the tank through the boundary layer and that all mass flow through the boundary layer will be driven to the surface by buoyancy forces. Mass is entrained into the boundary layer and transported to the surface of the liquid where it forms a warm, well mixed stratum at a uniform temperature that varies with time. Boundary layer flow is driven by a constant wall temperature that is hotter than the liquid bulk, which yields a mass flow rate into the stratum, Equation 5, as well as the temperature of the stratum, Equation 6:

$$\dot{M}_{\Delta} = \frac{4hA_{HC}}{\rho c_p} \tag{5}$$

$$\theta = \int_0^t \frac{qA_H dt}{\rho c_p V_{\Delta}} \tag{6}$$

This simplified model captures the general physical phenomenon of thermal stratification using mass and energy balances, however it has several limitations including the lack of a temperature profile within the stratum. The actual stratum layer would have a temperature profile with the hottest liquid on the surface. The model also does not take into account any interaction between the liquid and the ullage gas adjacent to it, which may be an important energy exchange mechanism depending on the conditions within the tank. Lastly, this model assumes there to be a constant and uniform wall temperature that drives the heating of the bulk liquid. For most situations, the tank will be exposed to a radiative heat flux resulting in a non-uniform wall temperature on the inside of the tank.

Tellep [11] also uses the boundary layer temperature and velocity profiles as analyzed in Eckert along with mass and energy balance into the boundary layer and stratum. The most significant differences between this model and the model presented by Bailey are the assumed one-dimensional stratum temperature profile, the buoyancy flow being driven by a constant heat flux instead of a constant temperature, as well as allowing for some energy exchange to the ullage gas from the stratum. This model yields expressions for the depth of the stratum and the surface temperature with time:

$$\frac{\Delta}{H} = 1 - \left[1 + 0.082(H/R)(Gr^*/\mathrm{Pr})^{2/7}\phi\right]^{-7} \tag{7}$$

$$T_s - T_b = \frac{2Hqt}{\rho c_p RI\Delta + L_v(\partial\rho/\partial T)_s RL} \tag{8}$$

In Equations 7 and 8, $\Phi = \nu t/H^2$, I is the non-dimensional energy integral, and L_v is the latent heat of vaporization.

Using the literature models presented by Bailey and Tellep, thermal stratification for various levels of reduced gravity, fluids and coast times was examined. It was found that because of the assumptions employed in the Bailey model, it consistently provided the shortest time to stratification and thus a worst case estimate. Using this model, Figure 3 shows the percent of cold bulk fluid remaining in the tank (that which has not been converted to warm stratum) as a function of time for LH_2, LOX, and LH_2O at two different reduced gravities, $g/g_0=10^{-2}$ and 10^{-4}. For each of the fluids, the tank will stratify faster with higher reduced gravity because the process is driven by buoyancy forces which increase proportional to the gravity. Stratification occurs more rapidly moving toward the lower left corner of the plot with water stratifying most quickly, followed by liquid hydrogen and then liquid oxygen.

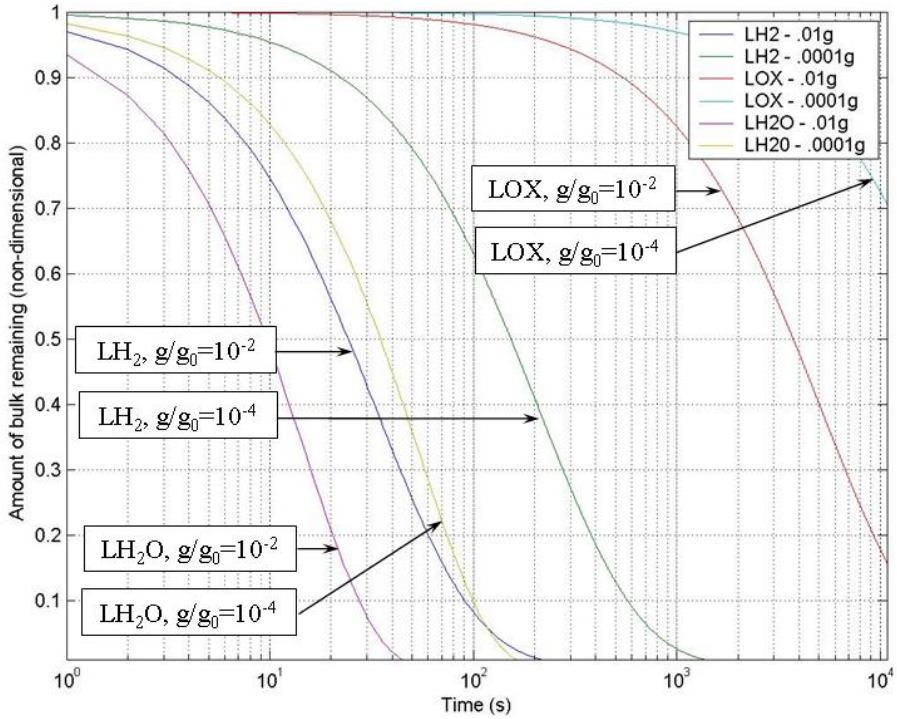

Figure 3: Plot of stratification with time for fixed ΔT=1 K and $g/g_0=10^{-2}$ and 10^{-4} for LOX, LH_2, and LH_2O. Stratification occurs more rapidly moving toward the lower left of the plot.

Figure 4 demonstrates the dependence of stratification on reduced gravity for LOX propellant.

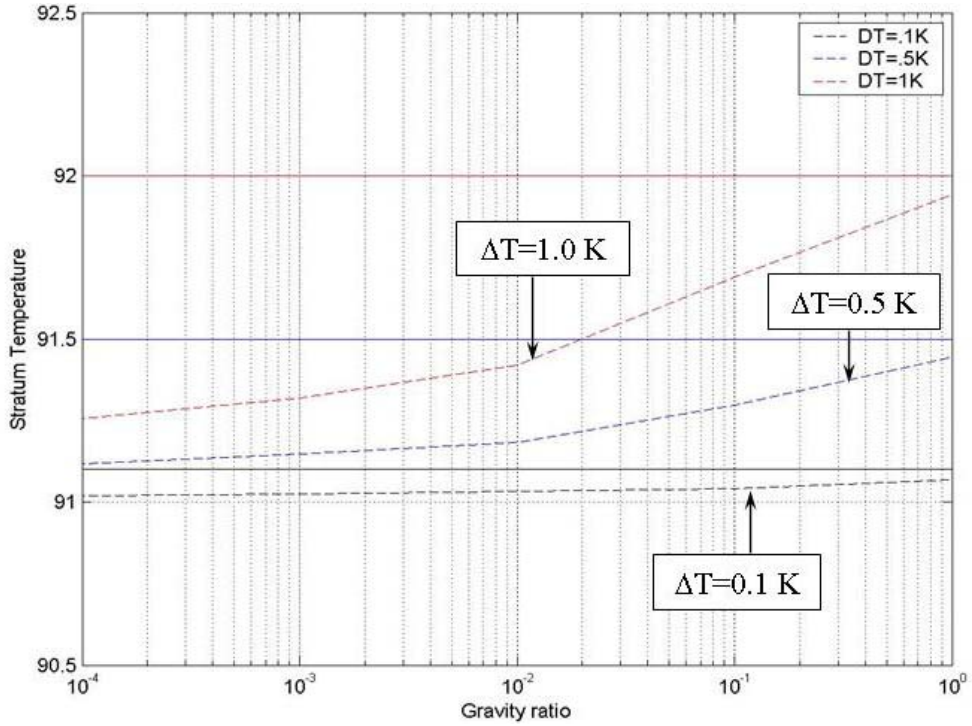

Figure 4: Plot of stratum temperature versus reduced gravity ratio as a function of tank wall and bulk temperature difference at 3 hours. LOX is initially at T_{bulk}=91 K.

The figure shows the temperature of the stratum at the end of a three hour coast as a function of reduced gravity ratio. Again the stratum is warmer for stronger gravity because of the physical dependence of buoyancy. There is also a strong dependence on the thermal properties of each liquid which results in the different rates of stratification demonstrated in Figures 3 and 4. In each of the cases, the hot wall temperature was chosen to be below the boiling temperature of the cryogens to simplify the heat transfer. In future simulations this assumption will be relaxed and boiling heat transfer modes will be included.

In order to achieve uniform thermal conditions, the upper stage is usually spun about its longitudinal axis at a rate of around 1degree per second. To capture the influence of tank rotation, a simplified analytical model was developed. When a contained volume of liquid is in steady-state, rigid body rotation the free surface will form a paraboloid of revolution. The model accounts for the change in shape by increasing the surface area being heated to include the height the liquid rises (along the walls) above the non-rotating case. This causes the liquid to heat up faster than when the tank is non-rotating due to increased heating area for the same volume of fluid. In order to arrive at a percentage of the bulk remaining at a given time, the model uses the vertex of the stratified parabola as the point of reference. Since the outlet for the propellant to the turbomachinery is typically located at the bottom-center of the tank, it is advantageous to determine the warmest temperature at that point. Figure 5 demonstrates results using liquid hydrogen and shows the percentage of bulk remaining at the vertex for a reduced gravity ratio of $g/g_0=10^{-3}$.

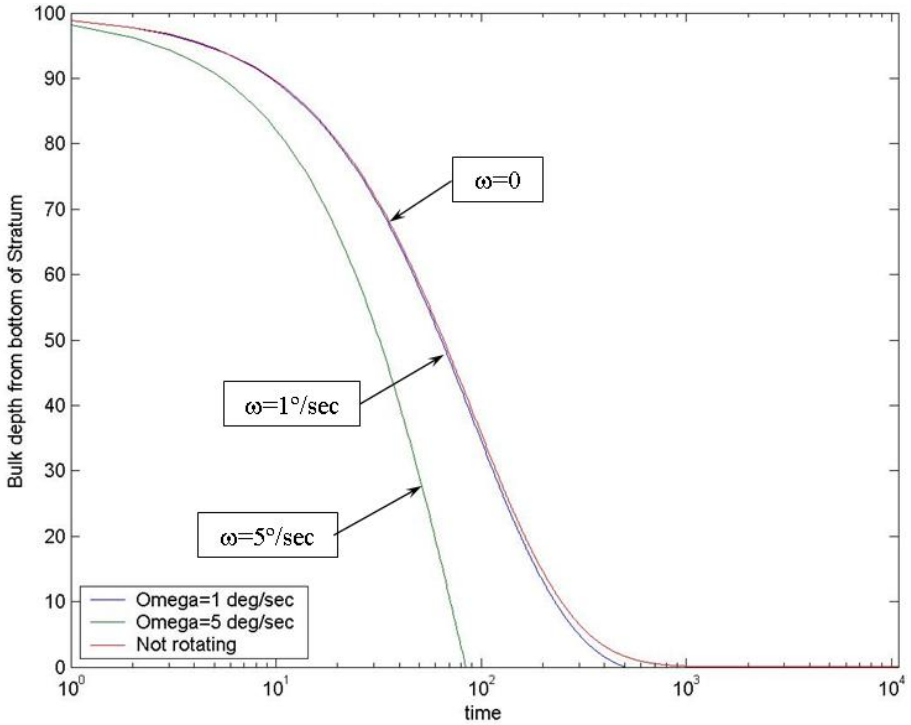

Figure 5: Bulk depth from bottom of stratum versus time for LH_2 as a function of tank spin rate about longitudinal axis for $g/g_0=10^{-3}$.

Keeping all other parameters constant, for higher rates of rotation, the liquid will stratify more quickly than the non-rotating case. However, it is important to note that for spin rates on the order of 1 °/s, the stratification versus time profile is essentially unaffected. However, if the spin rate is increased to 5 °/s the shape of the free surface is significantly altered and the stratification may proceed much more quickly.

The analytical models provide useful approximations but assume steady-state, solid body rotation and a fully established boundary layer. However, both time scales may be a significant fraction of the total coast time for low reduced gravity ratios. For example, it may only take ten seconds for the boundary layer to reach steady-state in high gravities, but it could take over an hour to reach steady-state when the gravity is lower than 0.1% of g_0. Low gravity also increases the steady-state time scale for a rotating liquid to achieve solid body rotation, which may also be on the order of an hour(s). Another feature not captured by the analytical models is the presence of secondary flow recirculation that is induced by the upward flow in the free convection boundary layer. This flow is then forced downward along the centerline of the tank, dragging warm stratified fluid with it. It is unlikely that this effect can be easily captured using simple analytical models as the magnitude of the recirculation zone, which is set by the density gradient, will vary with time. For this reason, simplified computational models have been developed to assess the importance of these effects.

3. Computational Modeling

The FLUENT CFD program was employed to investigate the affect of physical phenomena not captured in the analytical models. For the rotational cases FLUENT is also used to determine the time scales required to achieve steady-state, solid body rotation as a function of the spin rate, reduced gravity, tank geometry and fill level.

3.1: Thermal Stratification Modeling

Uniform and non-uniform structural grids were created in GAMBIT to optimize computational time and accuracy. Preliminary results indicate that the formation of the stratified layer in a mesh with a boundary layer scheme is similar to that of uniform mesh, although the non-uniform grids often require much greater computational time. Average CPU time to complete 100 time steps for the non-uniform mesh is about 8 hrs, while the simplified uniform mesh takes around 2.5 hrs. After a grid resolution study a 38 by 38 uniform mesh was used to study a laminar flow free convection case. A coupled second order implicit solver is used and flow equations and Reynolds stress equation are simulated with a first order upwind scheme. Turbulence kinetic energy and turbulence dissipation rate are computed using the QUICK scheme. The scheme takes weighted average of second order upwind and central interpolations, [4]. The Courant Number is set to 0.5. The criterions for the convergence remain default; 10^{-6} for the energy equation, 10^{-3} for the continuity, velocity and turbulence components.

In addition to the laminar cases, the flow within the 2-D cavity will be turbulent if $Ra > 10^9$, and these represent more likely cases for the actual spacecraft. To capture the flow a RNG turbulence model with enhanced wall function and full buoyancy effect is chosen while a Boussinesq approximation computes the flow due to buoyant force. Initial conditions for turbulence kinetic energy and turbulence dissipation rate are 0.01 m^2/s^2 and 0.01 m^2/s^3, respectively. Also a pseudo initial velocity of 10^{-10} m/s is added in the vertical direction, which helps initial convergence. This artificial velocity causes some fluctuations at the beginning of the simulation, but is quickly washed out by the free convective flow.

Figure 6 provides an example using CFD to capture the effects of stratification for liquid water in a square tank. Each of the figures is a temperature contour plot. In each case there is a 5 K temperature difference between the wall and the bulk fluid, and the lower wall is maintained at a temperature equal to the initial bulk temperature. The three columns represent three reduced gravity levels, g/g_0=1, 0.1, and 0.01 proceeding from left to right. Each horizontal row represents a fixed time. The non-dimensional Rayleigh number for these simulations was selected to be in the laminar range and is $Ra=7.5x10^3$ for all cases.

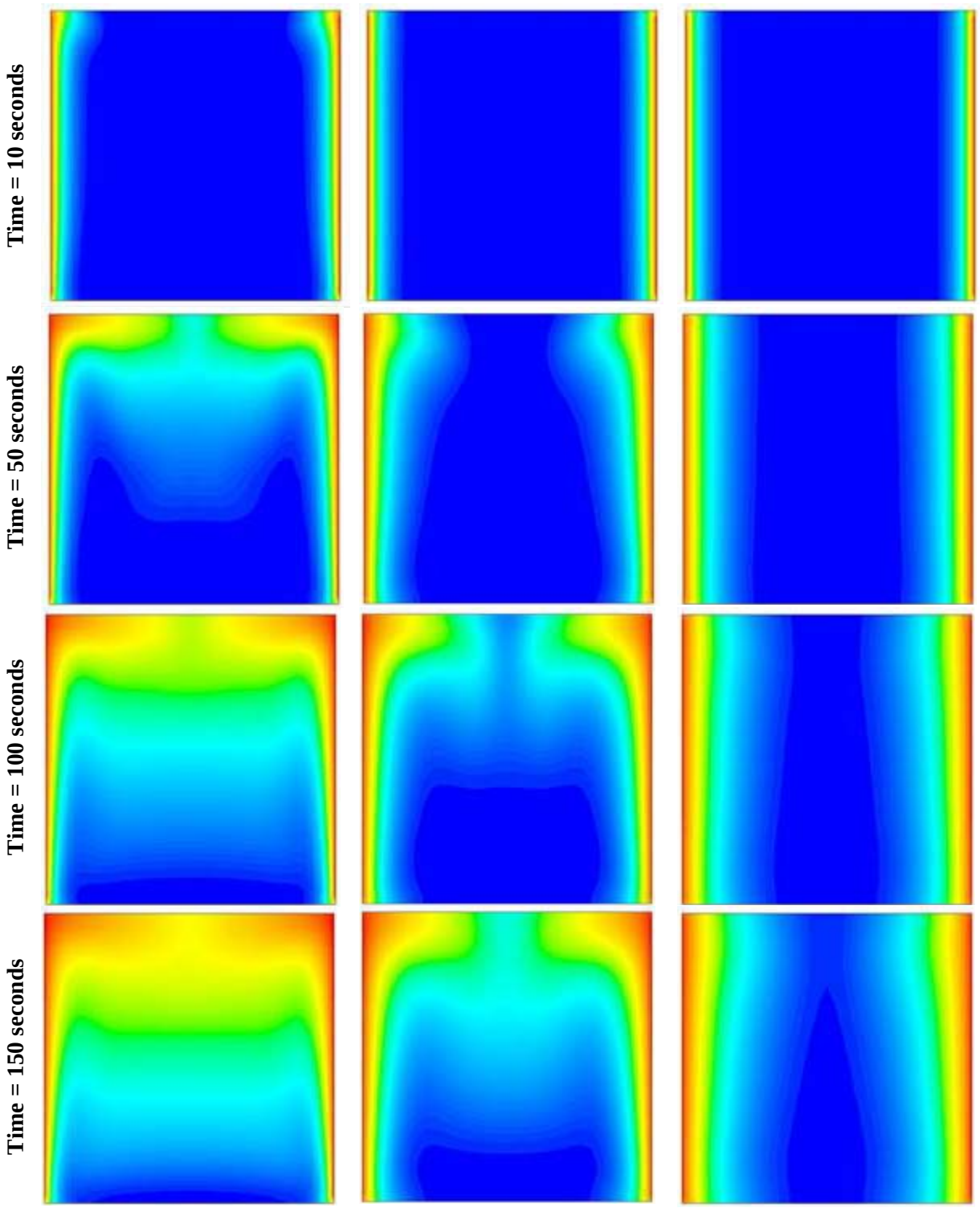

Figure 6: Example of CFD calculations for H_2O stratification. Ra=7.5x10^3, indicating a laminar flow. The three columns represent three levels of reduced gravity, g/g_0=1, 0.1, and 0.01. The difference between wall temperature and bulk fluid temperature is 5 K. The lower surface is maintained at constant temperature equal to the initial bulk temperature.

The temperature contour plots of Figure 6 show the same trends as the analytical models, but with an increased level of detail of the actual flow field. For the high gravity case, the thermal stratification is clear and envelops more than half the tank at 150 seconds. Conversely, at a reduced gravity level of 0.01, there is essentially no vertical stratification after 150 seconds. Similar trends are observed using the analytical models, but the assumption of a uniformly mixed and uniform temperature stratum lacks the fidelity that may be obtained from the CFD simulation. The plots also show that there are multiple ways to define the thermal stratification, for example if the bulk has changed by 0.1 or by 0.5 K.

3.2 Rotational Flow Modeling

As an effort to validate the preliminary rotational model, CFD has been employed to simulate liquid in a rotating tank. Preliminary cases have been completed using water in a square tank over a range of rotation rates and reduced gravity levels. Figure 7a shows an example of a comparison between the computational case and the analytical expression for the free surface of the parabola, which is given by Equation 9.

$$h = \frac{\omega^2 R^2}{2g} \qquad 9$$

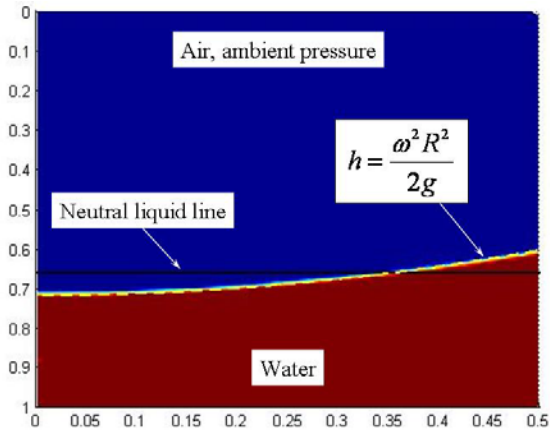

Figure 7a: Example of CFD simulation to capture effect of rotation. Figure shows right half of a square tank as well as the neutral liquid line (non-rotating). The tank is spinning at w=3 rad/sec and the reduced gravity level is 1. Agreement with the analytical parabolic shape is also shown.

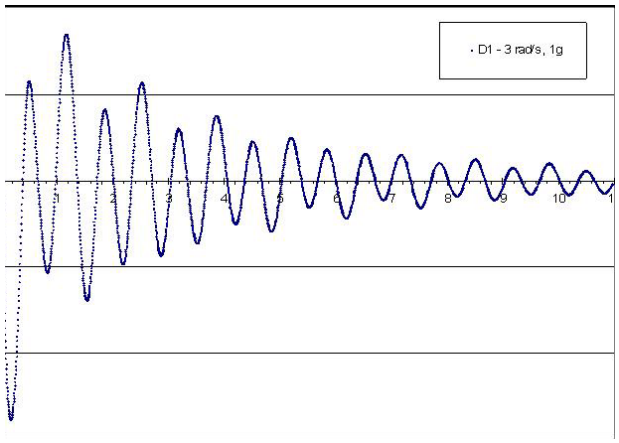

Figure 7b: Example of velocity oscillations during time to establish steady-state, rigid body rotation as the gravitational and centrifugal forces balance each other. The velocity is measured at a point in the liquid phase and is shown to shown to decay to near zero after about 10 seconds.

In Figure 7a the reduced gravity is set to 1 and the spin rate is 3 radians/second, or 171 º/sec. The numerical solution agrees well with Equation 9. This high spin rate was chosen so that these conditions could also be duplicated in the laboratory. Cases have also been simulated where the vertex of the parabola extends beyond the lower surface of the propellant tank.

Computational simulations also predict the time required for liquid in a rotating tank to reach a steady state. When the container is impulsively set into motion there as an imbalance between the gravitational and centrifugal forces, which results in an oscillatory behavior of the liquid. As time progresses these forces equilibrate and a steady-state, solid body shape is achieved. Figure 7b shows the time history of the velocity magnitude of a point located in the liquid, below the

free surface. For the case shown in Figure 7a, the velocity is seen to damp quickly and approach zero after about 10 seconds. However, simulations performed with a low reduced gravity take much longer to reach a steady state, and for reduced gravities on the order of 10^{-5} and spin rates of 1 º/sec., the steady-state time scale is on the order of hours. The implications of this oscillatory motion are that thin layers of the cryogenic propellant may be thrown against the hot internal tank surfaces leading to rapid boil off and a change in pressure within the tank. Consequently this change in pressure may lead to venting of the propellant resulting in less total propellant available at the conclusion of the coast phase. The spacecraft's settling thrust at the initiation of the orbital coast should keep the gravity levels moderately high which will encourage relatively rapid formation of the steady-state free surface parabola.

Future Work

The initial work presented here utilized a constant wall temperature, whereas the spacecraft tank walls are heated with a constant solar heat flux. The numerical simulations will be also examined with a constant heat flux and compared to the analytical predictions. The combined effects of stratification and rotation have not been explored in the numerical simulations. The next step is to combine the rotation and free convection cases into a single, time-dependent CFD model in order to capture the coupling of the rotation and the free convection. Some repression of the boundary layer as a result of the outward centripetal force may be expected, which could diminish the stratification but may also augment the heat transfer. These affects are not addressed in the analytical model introduced in this paper. Additional CFD work is to include spherical end caps on the tank to examine how the free convection is altered by a curved surface. Splash baffles and an isogrid will also be added on the internal walls of the tank to determine their potential impacts on propellant behavior during rotation and stratification.

Other effects which will be analytically modeled include nucleate and film boiling within the boundary layer and energy exchange with the ullage along the free surface of the stratum. Boiling is expected to occur at some point during the coast phase due to the thin layers of fluid near the wall. Spacecraft reorienting maneuvers resulting in fluid slosh also represent situations when boiling is likely to occur.

Summary and Conclusions

To ensure proper operation of upper stage engine turbomachinery after an orbital transfer coast, accurate modeling of the thermodynamic state of the propellants is needed. This paper serves as an introduction for examining various levels of analytical and computational models to capture a wide array of physical processes that may be taking place inside the cryogenic propellant tanks. The focus of initial efforts has been to examine thermal stratification and thermal conditioning of the stage through rotation about the spacecraft's longitudinal axis.

While the analytical models available in the literature capture important trends associated with thermal stratification, CFD may be used to examine a much greater level of detail, including the free convection boundary layer establishment time scales and the effect of secondary flows within the bulk fluid. For a rotating tank at various reduced gravity levels and rotational rates, CFD may be used to estimate the time scale necessary to achieve steady-state, solid body rotation. For low reduced gravity cases around $g/g0=10^{-4}$, this time scale may be on the order of an hour. This paper also introduced a simple extension of the literature models to include first order effects of spacecraft rotation on thermal stratification. The model indicates that at a reduced gravity ratio of 10^{-3} and a rotation rate of 1º/sec. there is little effect on thermal stratification relative to the non-rotating case. However, if the gravity level is lowered or the rotation rate increased, the time for stratification of the fluid may be significantly reduced. Furthermore there exists the potential for throwing all the liquid to the walls and leaving a dry area at the base of the tank where the inlet to the turbomachinery is located.

References

1. Bailey, T., VandeKoppel, R., Skartvedt,D., Jefferson, T., Cryogenic Propelllant Stratification Analysis and Test Data Correlation. AIAA J. Vol.1, No.7 p 1657-1659,1963.
2. Birikh, R.V.: Thermo-Capillary Convection in a Horizontal Layer of Liquid. Journal of Applied Mechanics and Technical Physics. No.3, pp.69-72, 1966
3. Eckert, E.R.G., Jackson, T.W.: Analysis of Turbulent Free-Convection Boundary Layer on a Flat Plate, Lewis Flight Propulsion Laboratory, July 12, 1950.
4. FLUENT 6.1 (2003) User`s Guide, Fluent Inc. USA.
5. Levich, V.G.: Physiochemical Hydrodynamics.Prentice Hall. 1962
6. Michalek, T. and T.A. Kowwalewski. "Natural Convection for anomalous density variation of water numerical benchmark," Progress in Computational Fluid Dynamics Vol.5, Nos.3/4/5. 2005.
7. Ostrach, S.; and Pradhan, A.: Surface-Tension Induced Convection at Reduced Gravity. AIAA Journal. Vol.16, No.5, May 1978.
8. Reynolds, W.C., Saterlee H.M.,: Liquid Propellant Behavior at Low and Zero g. The Dynamic Behaviour of Liquids, 1965.
9. Ruder, M.J., Little, A.D., Stratification in a Pressurized Container with Sidewall Heating. AIAA J. Vol.2, No.1 p 135-137, 1964.
10. Seebold, J.G.; and Reynolds, W.C.: Shape and Stability of the Liquid-Gas Interface in a Rotating Cylindrical Tank at Low-g. Tech. Rept. LG-4, Dept. of Mech. Engineering, Stanford University, March 1965.
11. Tellep, D.M., Harper, E.Y., Approximate Analysis of Propellant Stratification. AIAA J. Vol.1, No.8 p 1954-1956, 1963. Schwartz, S.H., Adelberg, M.: Some Thermal Aspects of a Contained Fluid in a Reduced-Gravity Environment, Lockheed Missiles & Space Company, 1965.
12. Yih, C.S.: Fluid Motion Induced by Surface-Tension Variation. The Physics of Fluids. Vol. 11, No.3, March 1968.
13. http://www.skyrocket.de/space/index_frame.htm?http://www.skyrocket.de/space/doc_sdat/goes-n.htm
14. http://www.boeing.com/defense-space/space/delta/delta4/d4h_demo/book01.html
15. http://www.spaceflightnow.com/news/n0201/28delta4mate/delta4medium.html

Acknowledgements

This work was supported through Analex agreement No. 05-001 under technical supervisor Jorge Piquero and program coordinator Eileen Gonzalez. Their support of this effort is greatly appreciated. The authors also wish to thank Mike Campbell and Martin Margulies for their technical input, advice and highly beneficial suggestions for improvement to this work.

Nomenclature

c_p	Specific heat at constant pressure, J/kg K
g	Gravitational acceleration, m/s^2
Gr	Grashof number
Gr*	Modified Grashof number, $g\beta qH^4/ \kappa \nu^2$
h	Heat transfer coefficient, $W/m^2 K$
H	Height of tank, m
L	Characteristic length scale, m
Nu	Nusselt number
Pr	Prandtl number
q	Heat flux, W/m^2
R	Radius of tank, m

β	Volumetric thermal expansion coefficient, 1/K
Δ	Depth of stratified region, m
δ	Boundary layer thickness, m
ΔT	Temperature difference, K
θ	Temperature difference in boundary layer, K
κ	Thermal conductivity, W/m K
μ	Viscosity, Ns/m^2
ν	Kinematic viscosity, m^2/s
ρ	Density, kg/m^3
ω	Spacecraft rotational spin rate, degrees/second